Early antitumor activity of oral Langerhans cells is compromised by a carcinogen

Yasmin Saba[a,1], Itay Aizenbud[a,1], Daniela Matanes[a], Noam Koren[a], Or Barel[a], Khalid Zubeidat[a], Tal Capucha[b], Eyal David[c], Luba Eli-Berchoer[a], Patrizia Stoitzner[d], Asaf Wilensky[e], Ido Amit[c], Rakefet Czerninski[f], Simon Yona[a,2,3], and Avi-Hai Hovav[a,2,3]

[a]Institute of Biomedical and Oral Research, Faculty of Dental Medicine, Hebrew University of Jerusalem, Jerusalem 9112102, Israel; [b]Department of Oral and Maxillofacial Surgery, Rambam Medical Care Center, Jerusalem 3109601, Israel; [c]Department of Immunology, Weizmann Institute, Rehovot 7610001, Israel; [d]Department of Dermatology, Venereology, and Allergology, Medical University of Innsbruck, Innsbruck A-6020, Austria; [e]Department of Periodontology, Hebrew University–Hadassah School of Dental Medicine, Jerusalem 9112102, Israel; and [f]Department of Oral Medicine, Sedation, and Maxillofacial Imaging, Hebrew University–Hadassah School of Dental Medicine, Jerusalem 9112102, Israel

Edited by Harvey Cantor, Department of Cancer Immunology and Virology, Dana-Farber Cancer Institute, Boston, MA; received October 13, 2021; accepted November 10, 2021

Early diagnosis of oral squamous cell carcinoma (OSCC) remains an unmet clinical need. Therefore, elucidating the initial events of OSCC preceding tumor development could benefit OSCC prognosis. Here, we define the Langerhans cells (LCs) of the tongue and demonstrate that LCs protect the epithelium from carcinogen-induced OSCC by rapidly priming αβT cells capable of eliminating γH2AX$^+$ epithelial cells, whereas γδT and natural killer cells are dispensable. The carcinogen, however, dysregulates the epithelial resident mononuclear phagocytes, reducing LC frequencies, while dendritic cells (DCs), macrophages, and plasmacytoid DCs (pDCs) populate the epithelium. Single-cell RNA-sequencing analysis indicates that these newly differentiated cells display an immunosuppressive phenotype accompanied by an expansion of T regulatory (Treg) cells. Accumulation of the Treg cells was regulated, in part, by pDCs and precedes the formation of visible tumors. This suggests LCs play an early protective role during OSCC, yet the capacity of the carcinogen to dysregulate the differentiation of mononuclear phagocytes facilitates oral carcinogenesis.

oral cancer | Langerhans cells | 4NQO

Oral squamous cell carcinoma (OSCC) is the most prevalent cancer in the oral cavity, representing about 90% of head and neck malignancies worldwide (1). Despite recent advances in the detection, prevention, and treatment of OSCC, this highly aggressive cancer, unfortunately, remains associated with a poor 5-y patient survival rate (2). This is attributed, in part, to the late diagnosis of OSCC, resulting in high mortality and morbidity rates. It is therefore crucial to understand the early events in the establishment of OSCC to improve the capacity to discover predictive markers and ultimately prevent tumor progression.

Langerhans cells (LCs) are a resident cell population of antigen-presenting cells (APCs) that exclusively occupy the stratified squamous epithelia, including the skin epidermis and the oral epithelium where SCC develops (3). Unlike skin epidermal LCs that arise from embryonic precursors immediately after birth and are self-maintained locally, oral LCs develop and are continuously replenished from circulating bone marrow (BM) precursors—predendritic cells (pre-DCs) and monocytes (4–6). Upon entering the lamina propria, LC precursors are exposed to BMP7, a member of the TGF-β1 superfamily that directs their translocation to the oral epithelium where local TGF-β1/ALK5 signaling drives their differentiation into LCs (7). Whereas skin LCs are considered a homogenous population, oral LCs can be further divided into at least three subsets: LC1 (CD11b^{low}CD103$^+$), LC2 (CD11b$^+$CD103$^-$), and monocyte-derived LCs (CD11b$^+$CD64$^+$). Despite such ontogenetic disparities within this population, epidermal and oral LCs share many similar transcriptomic signatures and immunological functions, suggesting that LCs can arise from various precursors in a tissue-dependent manner (3, 7).

Due to their epithelial location, LCs are thought to be the first APCs to encounter and react against early carcinogenic events. Nevertheless, previous studies have generated contradicting evidence for both epidermal and oral LCs during skin and oral SCC, respectively. Whereas epidermal LCs were reported to have antitumor activity in a carcinogen-induced skin SCC (8, 9), other studies found a deleterious impact of LCs in this disease (10, 11). The role of oral LCs in OSCC also remains elusive since our current knowledge relies on observational human studies, suggesting both an anti- and protumor role for these cells. Several studies have demonstrated reduced numbers of oral LCs in human OSCC (12–14), while elevated numbers compared to normal tissues were reported by others (15, 16). In oral epithelial dysplasia (OED), an oral pathology with a potential to become malignant, LC numbers increase with the severity of the OED lesions, but were significantly

Significance

Oral cancer is often diagnosed at late stages, resulting in a poor prognosis of this disease. Understanding early carcinogenic events taking place during the development of oral cancer is, therefore, an important unmet clinical need. This study identifies an early anticancer protective role of oral Langerhans cells (LCs), the principal mononuclear phagocyte involved in immunosurveillance of the oral epithelium. Continuous exposure to the carcinogen 4NQO hampers the local differentiation of LCs, while other mononuclear phagocytes and T cells with immunosuppressive characteristics populate the epithelium, leading to the development of oral cancer. These findings reveal an initial step by which immunosurveillance is compromised by a carcinogen, which could facilitate novel diagnostic approaches to better detection of oral cancer.

Author contributions: Y.S., T.C., P.S., A.W., R.C., S.Y., and A.-H.H. designed research; Y.S., I. Aizenbud, D.M., N.K., K.Z., and L.E.-B. performed research; I. Amit contributed new reagents/analytic tools; Y.S., I. Aizenbud, O.B., and E.D. analyzed data; and S.Y. and A.-H.H. wrote the paper.

The authors declare no competing interest.

This article is a PNAS Direct Submission.

[1]Y.S. and I. Aizenbud contributed equally to this work.

[2]S.Y. and A.-H.H. contributed equally to this work.

[3]To whom correspondence may be addressed. Email: s.yona@mail.huji.ac.il or avihaih@ekmd.huji.ac.il.

This article contains supporting information online at http://www.pnas.org/lookup/suppl/doi:10.1073/pnas.2118424119/-/DCSupplemental.

Published January 10, 2022.

reduced in lesions with malignant transformation (17). Yet, the numbers of LCs reported being either increased (18) or reduced (19) in OSCC compared to OED. The presence of oral LCs in the tumor microenvironment was further suggested to reflect a better prognosis for head and neck SCC patients in terms of cancer recurrence (20, 21). This correlation was also described with regards to laryngeal SCC in which LC infiltration was associated with longer disease-free survival (22, 23). While this suggests a protective role of LCs in established tumors, how LCs respond during the early events of carcinogenesis in the oral mucosa remains ill defined. Using a murine model of carcinogen-induced OSCC mimicking the disease in humans (24), this study reveals a protective role for LCs during the initial stage of OSCC. The carcinogen, however, rapidly alters the resident pool of mononuclear phagocytes residing in the oral epithelium, which display an immunosuppressive phenotype facilitating the development of a large T regulatory (Treg) population in the epithelium and subsequently tumor establishment.

Results

Characterization of LCs in the Tongue Epithelium. Exposure of mice to the carcinogen 4-nitroquinoline 1-oxide (4NQO) in the drinking water is known to induce OSCC in the tongue epithelium (25). Therefore, before embarking on changes in the tongue epithelium during oral tumor pathology, we first characterized the tongue mononuclear phagocyte compartment at steady state. Visualization of mononuclear phagocytes by immunofluorescence staining revealed a dense network of major histocompatibility complex class II (MHCII) and langerin-labeled cells, situated within the basal epithelial layers between the papillae, while extending their dendrites around each papilla (Fig. 1*A* and *SI Appendix*, Fig. S1*A*). Using flow cytometry, it became apparent that the majority of tongue epithelial MHCII$^+$CD11c$^+$ cells express the LC markers EpCAM and langerin (Fig. 1*B*). Some of these cells were EpCAM$^+$langerin$^-$, representing developing LCs as previously reported (4). Resident tongue LCs are predominately composed of the LC2 subset CD11b$^+$CD103$^-$ or CD24$^+$Sirp-α$^+$, while the frequencies of LC1 were low (Fig. 1*C*). To determine the abundance of monocyte-derived LCs, *Ms4a3^{Cre}-Rosa^{TdT}* mice were used, which simply fate map cells arising directly through the committed granulocyte-monocyte precursors (GMPs) expressing the tdTomato reporter gene (26). The analysis of these mice revealed that about 20 to 30% of tongue LCs derive from monocytes (Fig. 1*D*). Nevertheless, virtually all LCs and EpCAM$^+$ APCs express ZBTB46, a transcription factor selectively expressed by conventional DCs but no other myeloid cells (27, 28) (Fig. 1*E*). A population of MHCII$^+$CD11c$^+$EpCAM$^-$langerin$^-$ and negative for ZBTB46 was recovered in certain experiments, likely representing macrophage contamination located within the lamina propria that was unintentionally picked up during the isolation. Careful separation of the tongue epithelium from the lamina propria indicated that LCs are restricted to the epithelium, while other langerin-expressing APCs are virtually absent in either compartment (Fig. 1*F*). Besides the LCs, the tongue epithelium also contains large populations of γδ and αβ T cells as well as a population of monocytes (*SI Appendix*, Fig. S1*B*). Taken together, these data suggest that LC2s, arising from both pre-DCs and monocytes, are the predominant APCs surveying the epithelium of the tongue at a steady state.

Oral LCs Inhibit the Establishment of OSCC. To investigate the role of LCs in experimental OSCC, langerin-DTR (diphtheria toxin receptor) mice were administered the chemical carcinogen 4NQO for 10 wk in the drinking water and simultaneously depleted langerin-expressing cells by weekly injections of diphtheria toxin (DT) (Fig. 2*A*). As shown in Fig. 2*B*, mice treated with 4NQO+DT developed tumors more rapidly than mice treated with 4NQO alone. No spontaneous tumors were observed in the control groups receiving DT injections or left untreated. Congruent with these results, only groups that were treated with 4NQO began to lose weight 6 to 8 wk after the treatment, whereas the coadministration of DT accelerated the weight loss (Fig. 2*C*). Clinical assessment, based on the appearance of the mice and their reaction to stimulation, performed 16 wk after the commencement of the experiment further demonstrated a lower clinical score in the 4NQO-treated mice while the lowest score was observed in the 4NQO+DT group (Fig. 2*D*). Quantification of the tumorigenicity in the tongues revealed higher numbers of tumors per tongue as well as a larger size of the principal tumors in the 4NQO+DT group in comparison to the 4NQO-treated mice (Fig. 2*E*). Histopathological assessments of the tumors based on the basal cells' invasiveness, thickness of the epithelium, and the heterochromaticity of the nucleus, confirmed the increased severity of the tumors in the group treated with DT in addition to 4NQO (Fig. 2*F*). Of note, depletion of LCs before the initiation of the 4NQO treatment also resulted in accelerated OSCC (*SI Appendix*, Fig. S2). These results suggest LCs perform a protective role during 4NQO-induced OSCC, postponing the establishment of the tumors.

LC-Mediated Immunity Eliminates γH2AX$^+$ Epithelial Cells. LCs are thought to be the first mononuclear phagocyte to encounter carcinogenic events in the oral epithelium to prime naive αβT cells; therefore, we examined the capacity of LCs to migrate to the lymph nodes (LNs) in the presence of 4NQO. To this end, the tongue epithelium was painted with a solution containing fluorescein isothiocyanate (FITC) and 4NQO to enable the tracking of LCs or DCs migrating to the LNs as these cells would be labeled with FITC. Indeed, a population of migratory FITC$^+$ LCs were detected in the cervical LNs 3 d after the FITC application (Fig. 3*A*). Interestingly, additional populations of EpCAM$^+$CD207$^-$ and EpCAM$^-$CD207$^-$ DCs were also labeled with FITC and detected in the LNs, indicating that other oral DC subsets can migrate to the LNs in this setting. In accordance with these observations, elevated levels of the LN homing chemokines, *Ccl19* and *Ccl21*, were detected in the tongue and the expression of adhesion molecules necessary for transendothelial migration via lymphatic vessels (Fig. 3*B*). Next, we examined the frequencies of CD8$^+$ and CD4$^+$ T cells in the tongue epithelium 1 wk after exposure to 4NQO in the drinking water. The relative frequencies of CD8$^+$ and CD4$^+$ T cells were significantly increased in the epithelium of the 4NQO-treated groups (Fig. 3*C*). However, depletion of LCs significantly reduced the abundance of these T cells, indicating that the early migration of LCs is crucial for T cell priming. Of note, the relative frequencies of epithelial γδT cells were reduced in 4NQO-treated mice due to the increase of αβT cells (Fig. 3*C*). To test whether the absence of LCs directly affects the numbers of cells undergoing DNA damage by the carcinogen, we stained the tongue epithelium of 1-wk 4NQO-treated groups with an antibody against the DNA damage marker γH2AX. γH2AX$^+$ cells were detected in the epithelium only upon exposure to 4NQO, while depletion of LCs significantly increased the number of these cells (Fig. 3*D*). Moreover, LC depletion up-regulated the expression of the stress-induced NKG2D ligands such as *Rae1* and *Ublp1* (Fig. 3*E*). Higher numbers of γH2AX$^+$ cells were also detected when NSG mice or *Rag1$^{-/-}$* mice were treated with 4NQO for 1 wk compared to wild-type mice, supporting the view that lymphocytes mediate the clearance of these cells (Fig. 3*F*). To assess the role of γδT cells in the elimination of DNA-damaged cells, we used the

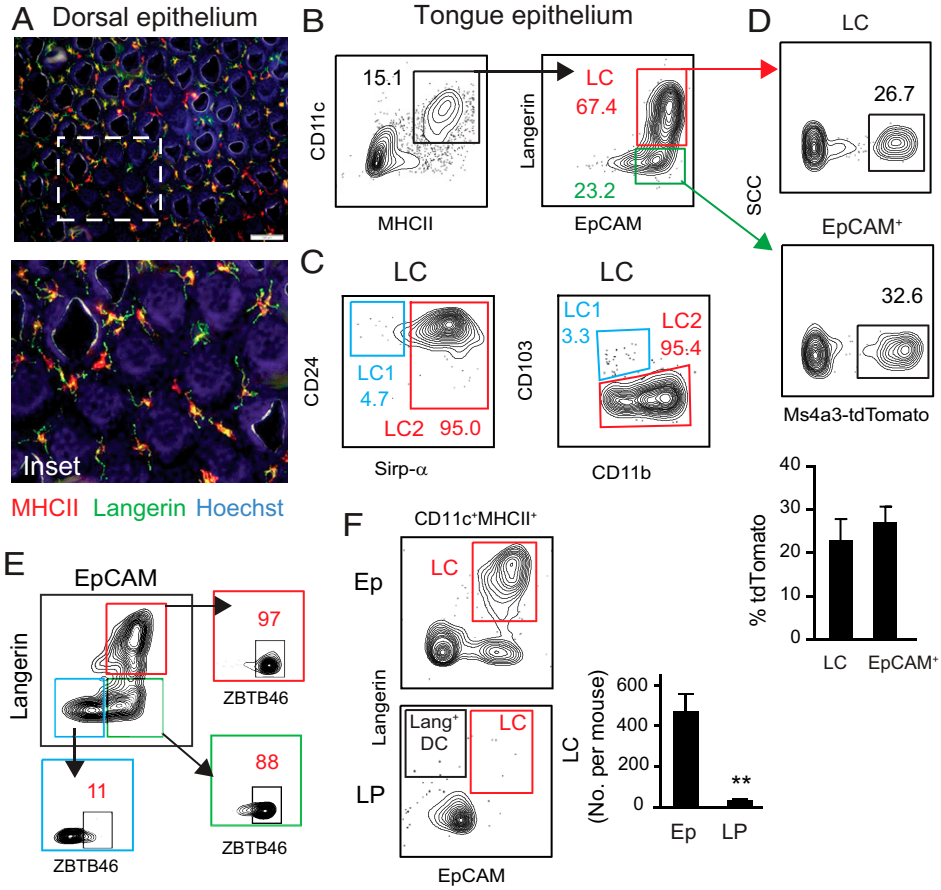

Fig. 1. Characterization of LCs in the tongue epithelium. (*A*) Immunofluorescence whole-mount staining from tongue epithelial layers of adult B6 mice with mAbs directed against MHCII (red), langerin (green), and with Hoechst (blue) for nuclear visualization. Representative image from four independent experiments. (Scale bar, 100 μm.) (*B* and *C*) Epithelial cells were prepared from the tongue of wild-type (WT) B6 mice and stained with the noted antibodies to identify by flow cytometry (*B*) epithelial mononuclear phagocytes (CD45$^+$CD11c$^+$MHCII$^+$) and LCs (EpCAM$^+$langerin$^+$ APC) as well as (*D*) the LC subsets based on CD24 and Sirp-α or CD103 and CD11b expression. Data are representative of three independent experiments. (*D*) Tongue epithelial cells were prepared from *Ms4a3^{Cre}-Rosa^{TdT}* mice and stained for LCs; the flow cytometry plots and graph present the mean frequencies + SEM of tdTomato$^+$ cells among LCs and EpCAM$^+$ APCs (n = 3). Data are representative of two independent experiments. (*E*) Tongue epithelial cells were prepared from *Zbtb46^{GFP}* mice and stained for LCs; the frequencies of GFP/ZBTB46-positive cells among LCs, Epcam$^+$ APCs, and EpCAM$^-$langerin$^-$ APCs are presented. Representative image from two independent experiments. (*F*) The epithelium and lamina from the tongue of WT B6 were separated and processed; the flow cytometry plots and graph present the mean percentages + SEM of cells expressing EpCAM and/or langerin among the CD11c$^+$MHCII$^+$ population in each tissue (n = 5). Data are representative of two independent experiments. Ep, epithelium; LP, lamina propria, $^{**}P < 0.01$.

Tcrd-GDL mice enabling the specific ablation of these cells upon administration of DT (29). Despite the absence of γδT cells, the numbers of γH2AX$^+$ cells remained unaffected, ruling out their involvement in cell clearance (Fig. 3*G*). Moreover, oral γδT cells, unlike their equivalents in the skin epidermis, do not express high levels of NKG2D (*SI Appendix*, Fig. S3). Since natural killer (NK) cells were previously shown to be rapidly recruited during skin carcinogenesis to eliminate DNA-damaged cells (9), we examined the presence of these cells in the tongue epithelium. As shown in Fig. 3*H*, NK cells could not be detected by flow cytometry in the tongue epithelium 48 h following the exposure to 4NQO. Taken together, these data suggest that LC-primed αβT cells, rather than γδT cells or NK cells, probably mediate the elimination of transformed epithelial cells early after exposure to the carcinogen.

4NQO Rapidly Reduces the Frequencies of Tongue Resident LCs. Since conditional ablation of LCs accelerates the development of carcinogen-induced OSCC, we asked what impact 4NQO has on tongue LCs. For this, B6 mice were treated with 4NQO in the drinking water, and the frequencies of tongue LCs were quantified over 5 wk before the detection of visible tumors. As depicted in Fig. 4*A*, the frequencies of total CD45$^+$ leukocytes in the tongue epithelium sharply increased from the first week of 4NQO treatment. In contrast, the frequencies of MHCII$^+$CD11c$^+$ cells among the total leukocytes decreased gradually, which contributed to the significant increase of other leukocytes such as the αβT cells. Nevertheless, LCs were considerably reduced during the first 3 wk and also remained low in the fifth week of the treatment (Fig. 4*A*). This was confirmed by immunofluorescence analysis, as clusters of MHCII$^+$ cells were detected in the epithelium, whereas staining for langerin was rare (Fig. 4*B*). Of note, constant exposure to the carcinogen was required to maintain the reduction of LCs, since the removal of 4NQO after a 3-wk treatment restored the LC population within 3 wk (Fig. 4*C*). As LC differentiation is driven by exposure to BMP7 and TGF-β1 (7), we asked whether 4NQO down-regulates the expression of these molecules. However, the mRNA levels of *Tgfb1* and *Bmp7* were either up-regulated or remained unchanged in the third wk of the 4NQO treatment, respectively, compared to the naive control (Fig. 4*D*). On a protein level, BMP7 and TGF-β1 were equally expressed in the tongues of both groups (Fig. 4*E*). We further quantified the mRNA of *Ccl2* and *Ccl20*, chemokines mediating the

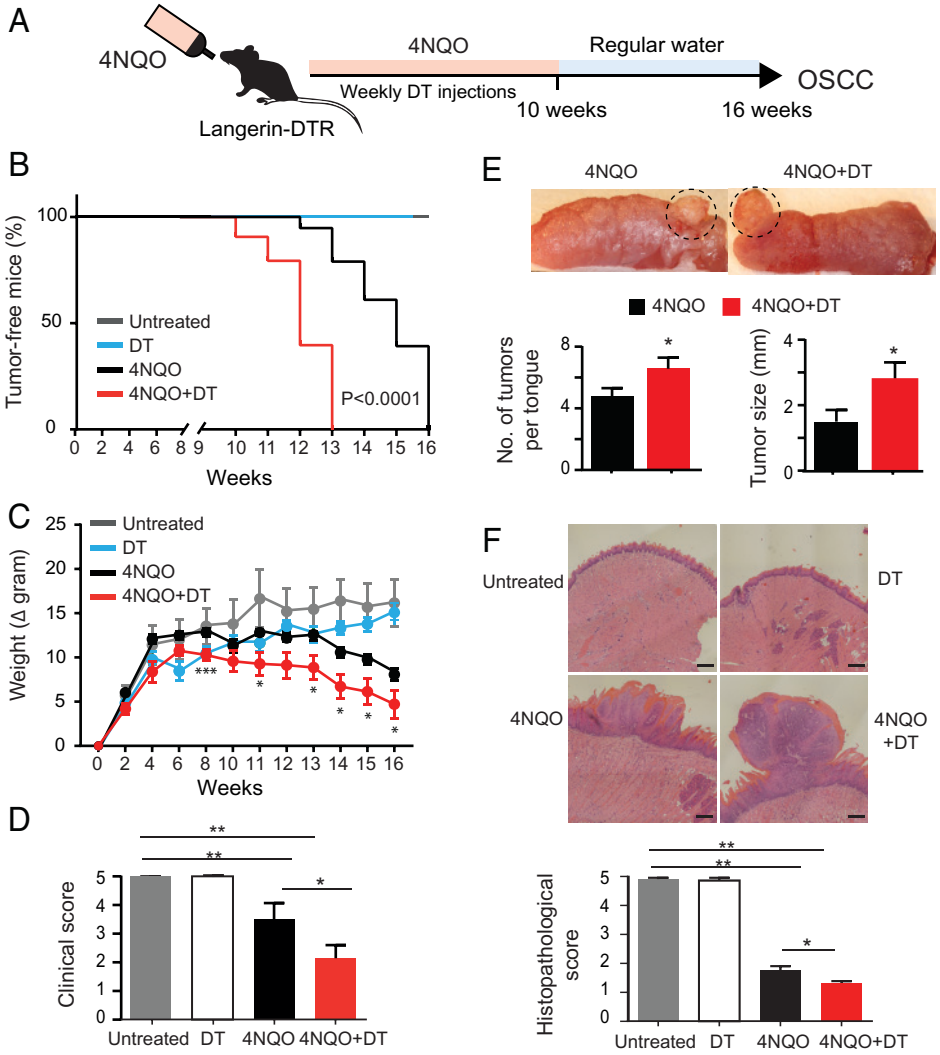

Fig. 2. Conditional depletion of LCs facilitates OSCC. (*A*) Illustration depicting the induction of experimental OSCC in *langerin-DTR* mice receiving 4NQO in the drinking water for 10 wk while administered with DT on a weekly basis. (*B* and *C*) Graphs show (*B*) the percentages of tumor-free mice and (*C*) the changes in the mouse weight + SEM since the beginning of the experiment ($n = 8$). Data are representative of two independent experiments. (*D*) The clinical score of the various experimental groups ($n = 8$). (*E*) Representative images of the tumors and graphs depicting the mean number of tumors per tongue + SEM and the mean size of the main tumors + SEM measured at the end of the experiment ($n = 6$ to 8). Representative image from four independent experiments. (*F*) Representative hematoxylin and eosin (H&E) histological sections of the tumors and/or the tongue epithelium. Graph shows the mean histopathological score + SEM of the various experimental groups ($n = 6$ to 8). (Scale bar, 50 μm.) Representative data from two independent experiments are shown. $^*P < 0.05$, $^{**}P < 0.01$.

recruitment of LC precursors into the epithelium. While *Ccl2* was not significantly alerted, *Ccl20* expression was decreased in 4NQO-treated mice compared to the control group (Fig. 4*D*). Next, we examined the capability of 4NQO to directly impair LC differentiation, by employing in vitro differentiation cultures in which BM cells are exposed to GM-CSF+TGF-β1 to drive the development of LCs. Using concentrations of 4NQO that do not broadly impact cell survival, the carcinogen did not interfere with the differentiation of LCs (*SI Appendix*, Fig. S4 *A* and *B*). Taken together, LCs are rapidly reduced in the tongue epithelium while other mononuclear phagocytes are likely recruiting and/or developing locally. The carcinogen is indirectly reducing the levels of LCs but this does not involve the dysregulation of BMP7 and TGF-β1 expression in the tissue.

Reprogramming of Tongue Epithelial Cells by Prolonged Exposure to 4NQO Contributes to the Impairment of LC Repopulation. To get insight into the impact of 4NQO on the tongue epithelial cells during the period in which LCs are reduced, we profiled the global gene expression of fluorescence-activated cell sorting (FACS)-sorted epithelial cells ($CD45^-$ cells) after 1 and 3 wk of 4NQO treatment and compared it to naive mice. The hierarchical clustering of the three cell populations, as well as principal component analysis (PCA), indicated a significant difference between the epithelial cells of naive and 4NQO-treated mice, as well as between epithelial cells sorted from mice treated with the carcinogen for 1 and 3 wk (Fig. 5 *A* and *B*). In agreement with the rapid DNA damage induced by the carcinogen, the analysis of gene set enrichment analysis (GSEA) revealed that cellular pathways involved in the cell cycle, DNA repair, and apoptosis, were up-regulated in epithelial cells treated with 4NQO for 1 wk and to a lesser extent for 3 wk (Fig. 5*C*). Exposure to 4NQO for 1 wk also significantly down-regulated the expression of genes related to innate immune sensing and function such as TNF-α signaling via NFκB, complement, and various TLR pathways. In the third week, however, the inhibition of immunological mechanisms was not observed and pathways related to the IFN-α, IFN-γ, and inflammatory responses were increased in the epithelial cells (Fig. 5*D*). TGF-β signaling in epithelial cells that is crucial for

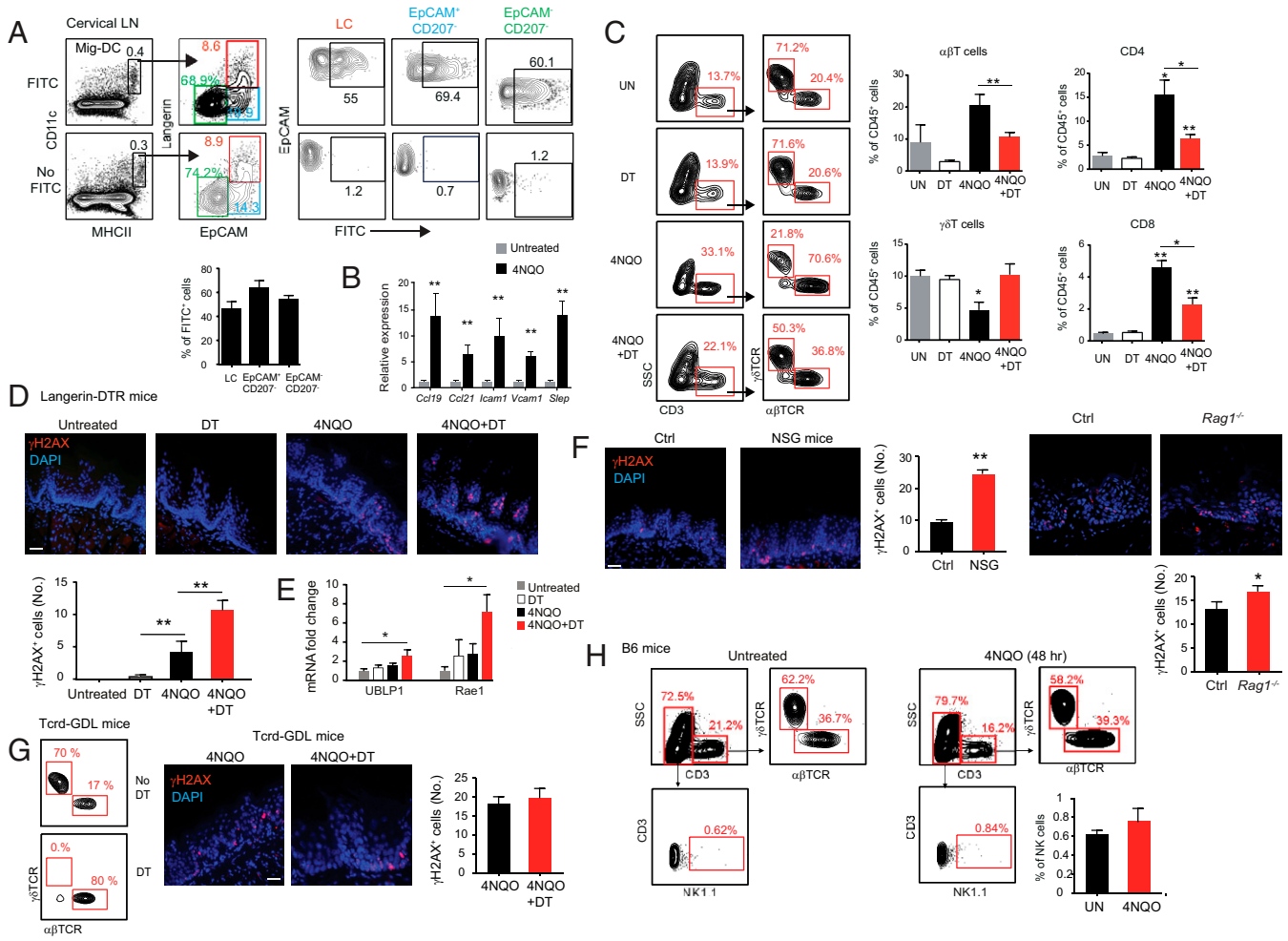

Fig. 3. LC-mediated immunity eliminates γH2AX$^+$ epithelial cells. (*A*) Flow cytometry analysis demonstrates the frequencies of FITC-labeled migratory (Mig.) LCs and other DC subsets (Mig. DCs) in the cervical LNs 24 h after applying FITC+4NQO solution on the tongue epithelium. The negative control group represents mice treated with 4NQO without FITC painting. Representative flow cytometry plots and graph from four independent experiments ($n = 3$ to 5). (*B*) Quantification of the expression of the noted genes in the tongue by RT-PCR presented as the mean values + SEM ($n = 5$). Representative data are from two independent experiments. (*C*) Representative flow cytometry plots and graphs present the mean frequencies + SEM of the various T cell subtests in the tongue epithelium 1 wk after the 4NQO treatment in the presence or absence of LCs. (*D*) Mice were treated with 4NQO in the drinking water for 1 wk. Immunofluorescence staining of tongue epithelial cross-sections were prepared from the various groups with mAbs directed against γH2AX (red) and with DAPI (blue). (Scale bar, 50 μm.) Graph shows the mean number + SEM of γH2AX$^+$ cells in the epithelium of each group ($n = 5$). Data are representative of three independent experiments. (*E*) Quantification of the expression of *Ublp1* and *Rae1* genes in the tongue epithelium 1 wk after the 4NQO treatment. Data are presented as the mean values + SEM ($n = 5$) and represent the data of three independent experiments. (*F*) Representative images and a graph show the mean numbers + SEM of γH2AX$^+$ cells in the epithelium of NSG mice or *Rag1*$^{-/-}$ mice versus control mice 1 wk after 4NQO treatment ($n = 5$). Data are representative of two independent experiments. (*G*) *Tcrd-GDL* were administered with DT to ablate γδT cells and then treated with 4NQO for a week. Representative flow cytometry plots demonstrate the depletion of γδT cells. Representative immunofluorescence images and a graph show the mean numbers + SEM of γH2AX$^+$ cells in the epithelium ($n = 5$). Data are representative of two independent experiments. (*H*) Flow cytometry plots and graph show the mean percentages + SEM of NK cells among CD45$^+$CD3$^-$ cells in the tongue epithelium of naive mice and mice treated with 4NQO for 48 h ($n = 4$). UN, untreated. (Scale bar, 50 μm.) *$P < 0.05$. **$P < 0.01$.

LC differentiation was reduced during the first but not the third week of treatment, in agreement with our earlier observations. Interestingly, 4NQO also down-regulated cellular pathways related to oxidative phosphorylation in the third but not the first week of exposure, which was the first-ranked down-regulated pathway in the analysis. To examine whether the reduction in the oxidative phosphorylation pathway can affect LC development, we differentiated LCs from BM cells in vitro in the presence of oligomycin, an inhibitor of adenosine triphosphate (ATP) synthase that reduces oxidative phosphorylation. Incubation of the differentiation cultures with 5 nM of oligomycin had limited effects on the viability of the differentiating cells and the overall frequencies of MHCII$^+$CD11c$^+$ cells in the culture (*SI Appendix*, Fig. S5 and Fig. 5*F*). Nevertheless, the generation of LCs (EpCAM$^+$langerin$^+$) and partially differentiating LCs (EpCAM$^+$langerin$^-$) were specifically reduced when the oligomycin was added. Collectively, these data demonstrate a fundamental alteration in the immunological response of the tongue epithelial cells to 4NQO early after the exposure. The carcinogen-induced down-regulated expression of the oxidative phosphorylation genes might represent a metabolic shift in the epithelium that potentially inhibits the differentiation of LCs.

Sustained Exposure to 4NQO Disrupts the Mononuclear Phagocyte Pool in the Tongue Epithelium. To probe the population of APCs developing in the tongue epithelium simultaneously with the decrease of LCs, *Zbtb46*^{gfp} mice were administrated 4NQO and analyzed. In contrast to LCs of naive mice that were positive to

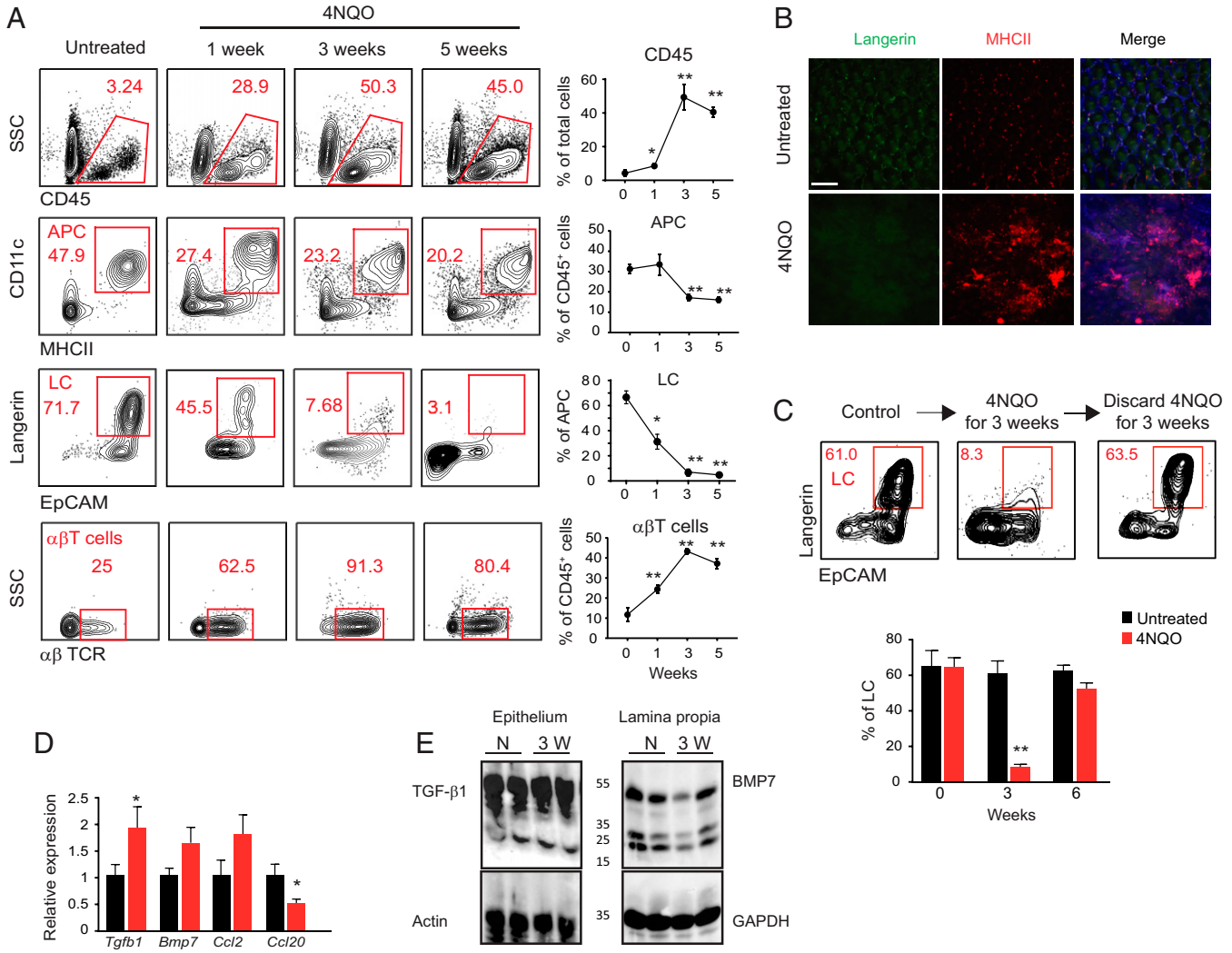

Fig. 4. Chronic exposure to 4NQO rapidly reduces the frequencies of tongue LCs. (*A*) WT B6 mice were administered 4NQO in the drinking water for 5 wk and the tongue epithelium was processed at the noted times for flow cytometry analysis. Representative flow cytometry plots and graph depict the mean frequencies + SEM of total CD45$^+$ leukocytes, APCs, LCs, and αβT cells ($n = 5$). (*B*) Immunofluorescence whole-mount images of epithelial layers prepared from naive or 4NQO-treated B6 mice (3 wk) stained with mAbs directed against MHCII (red), langerin (green), and with DAPI (blue). Representative image from three independent experiments. (Scale bar, 100 μm.) (*C*) B6 mice were treated with 4NQO in the drinking water for 3 wk; the 4NQO was then removed and the mice were provided with regular water for 3 additional weeks. Representative flow cytometry plots and graph present the frequencies + SEM of LCs in the tongue epithelium at the indicated times ($n = 5$). Representative data are from three independent experiments. (*D*) RT-PCR quantification of the expression of the noted genes in the tongue of naive B6 mice or mice treated with 4NQO for 3 wk. Data are presented as the mean expression values + SEM ($n = 5$). Representative results are from two independent experiments. (*E*) Western blot analysis showing the presence of TGF-β1, BMP7, ACTIN, and GAPDH in the epithelium and lamina propria of tongue tissue of B6 naive mice or mice treated with 4NQO for 3 wk ($n = 3$). *$P < 0.05$. **$P < 0.01$.

ZBTB46 (including the monocytes-derived CD64$^+$ LCs), the APCs of 4NQO-treated mice segregated into ZBTB46$^+$CD64$^-$ and ZBTB46$^-$CD64$^+$ subsets, likely representing DC and macrophage populations, respectively (Fig. 6*A*). Next, single-cell RNA-sequencing analysis (scRNAseq) was performed on enriched CD45$^+$ cells prepared from the tongue epithelium of wild-type mice treated or not with 4NQO. The tissues were collected from mice treated with 4NQO for 5 wk since at this time point the shift in epithelial leukocytes has been established. We used the MetaCell algorithm (30) to identify homogeneous and robust groups of cells from scRNAseq data. We retained a single-cell transcriptome for 4,667 cells after removing doublets and dead cells during initial quality control. Various myeloid (DCs, monocyte-derived APCs, mast cells, and neutrophils) and lymphoid (αβT cells, γδT cells, and NK cells) leukocytes were identified in the tongue epithelium, as well as epithelial cells that were not removed by the enrichment (Fig. 6*B*). Of note, the epithelium of untreated mice contains fewer subsets of leukocytes that consist of LCs, αβT cells, γδT cells, and a few NK cells (Fig. 6*C*). In line with the above results, the APC population expressing *Cd74* (also *H2-Aa*/*Ab1*/*Eb1*) and *Itgax*/CD11c consists of two main clusters representing macrophages and DCs (Fig. 6 *D* and *E*). The monocyte-derived macrophages express the signature genes such as *Ms4a7*, *Cx3cr1*, *Mafb*, and *Adgre1* (F4/80). Within the macrophage population, three main clusters were further characterized: *Ccl5*^{hi}*Ifitm3*^{hi} subset (*Igs15*, *Cxcl9*^{hi}, and *Ccl4*), *Trem2*^{hi}*Apoe*^{hi} subset (*Cxcl9*$^+$ and *Mt1*), and a subset expressing *C1q*^{low}*Cebpb*$^+$ (*Plac8* and *Ly6c2*) (Fig. 6*F*). Of note, expression of *Trem2*, *Apoe*, and *Ccl5* is associated with the capacity of macrophages to induce an immunosuppressive microenvironment and to facilitate carcinogenesis and metastases (31–33). Moreover, virtually all the macrophages express high levels of *Tgfbi* (TGF-β–induced protein), previously proposed to have a protumor role in OSCC (34, 35). The DC

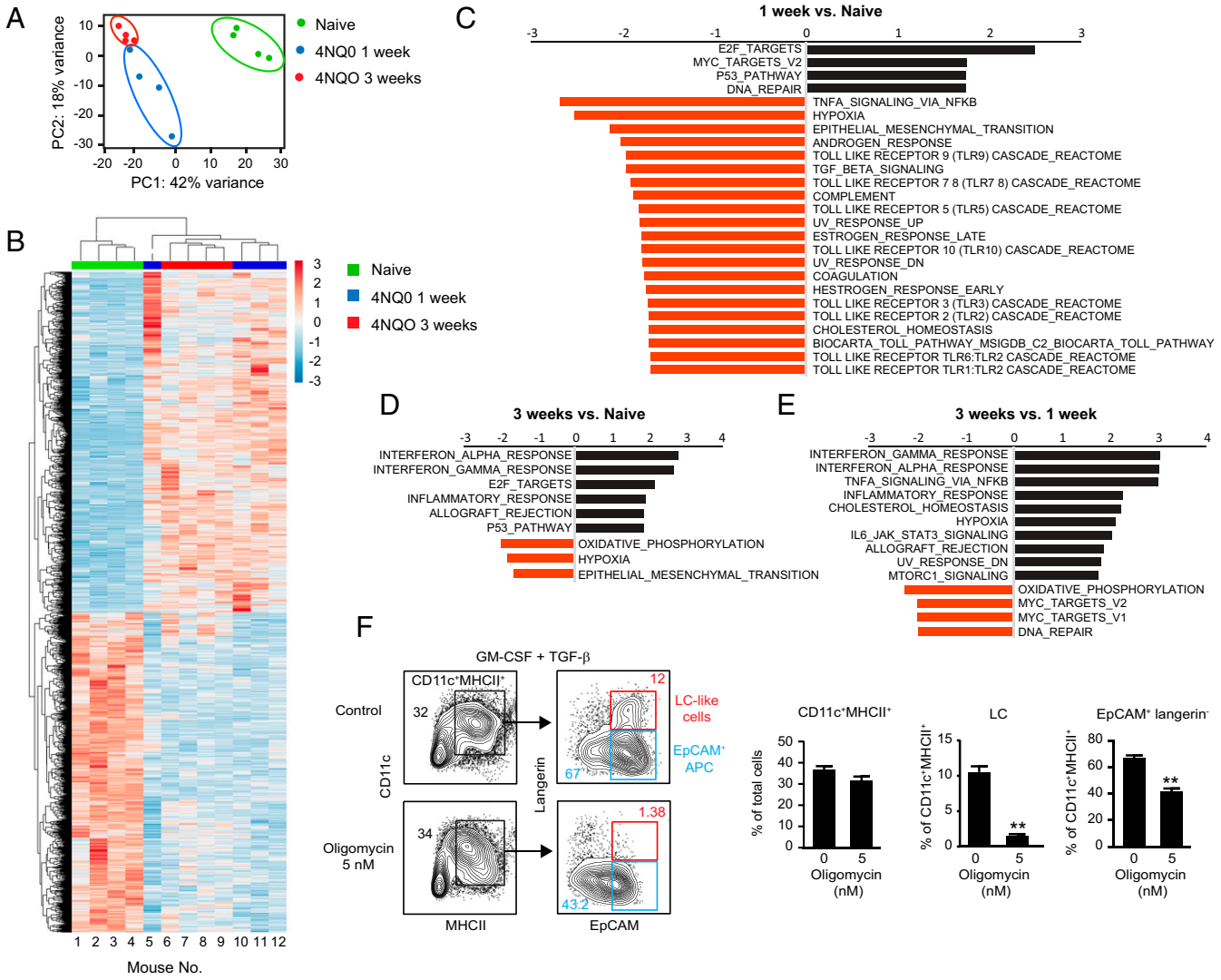

Fig. 5. 4NQO induces a shift in the transcriptomic signature of tongue epithelial cells. Epithelial cells were sorted from naive B6 mice and mice treated with 4NQO for 1 or 3 wk and subjected to global gene expression analysis. (*A*) PCA of the most variable transcripts expressed by the different epithelial cell subsets. (*B*) Hierarchical clustering of the genes differentially expressed in the naive and the 4NQO-treated epithelial cells. (*C–E*) Significantly up-regulated and down-regulated gene pathways identified by GSEA analysis among the various groups of epithelial cells (familywise error rate [FWER] <0.05). (*F*) BM cells were cultured for 5 d with GM-CSF and TGF-β to drive the differentiation of LCs in the presence or absence of 5 nM oligomycin. Flow cytometry plots and graphs show the frequencies of CD11c$^+$MHCII$^+$ cells, LCs (EpCAM$^+$ langerin$^+$), and partially differentiated LCs (EpCAM$^+$ langerin$^-$) as the mean values + SEM ($n = 3$). Representative results are from three independent experiments. $^{**}P < 0.01$.

populations were more complex and various clusters were detected (Fig. 6 *E* and *G*). A subset of the DCs express *Irf8*, *Ccr7*, *Ccl22*, and *Socs2*, suggesting that these are migratory DCs. Expression of CCL22 and SOCS2 by DCs was previously shown to promote the priming of Treg cells and to block antitumor immunity (36, 37). We further confirm the ability of these relatively late migratory DCs to reach the LNs, though at lower frequencies than LCs/DCs migrating after a 1-wk treatment with 4NQO (*SI Appendix*, Fig. S6 *A* and *B*). Direct quantification of CCL22 in the tongue epithelium reveals high expression from the first to the fifth week of 4NQO treatment (*SI Appendix*, Fig. S5*C*). Another cluster of DCs express *Siglech*, *Ly6d*, *Ccr9*, *Fcrla*, *Cd7*, *Irf8^{hi}*, *Ly6c2*, and *Cox6a2*, indicating the presence of plasmacytoid DCs (pDCs) in the tongue epithelium at this period. Besides these two subsets, the largest DC cluster expresses *Epcam*, a marker known to be first expressed by LC precursors in the course of their differentiation into LCs (7). The major subset of *Epcam*$^+$ DCs (*Ifitm3*, *Fcerg1*, *Cd72*, and *Ifitm1*) did not express *Cd207*/langerin, while some cells were proliferating (*Top2a* and *Mki67*). Other *Epcam*$^+$*Cd207*$^-$ DCs clustered into three subsets: 1) *Cxcl9*, *Irf8*, *Xcr1*, *Ifitm3*, *Isg15*, *Itif1*, and *Itif3*; 2) *Xcr1*, *Irf8*, *Cd9*, and *Itgae* (CD103); and 3) *Cd209a*, *Cd7*, *Ifitm3*, and *Fcerg1*. This large *Epcam*$^+$*Cd207*$^-$ DC population is likely representing partially or aberrantly differentiated LCs. Nevertheless, in line with the earlier flow cytometry analysis, minor subsets of LCs were detected in the epithelium that express *Epcam*, *Cd207*, Cd9, *Itgam* (CD11b), *Mfge8*, *Cd72*, and *Adgre1* (F4/80) representing LC2, and *Epcam*, *Cd207*, *Xcr1*, *Sirpa*, *Irf8*, and *Mfge8* that signify LC1. Interestingly, a population of cells expressing both LC- and neutrophil-associated genes (*Epcam*, *Cd207*, *Lyz2*, *Camp*, *Ngp*, *S100a8/9*, *Lcn2*, *Chil3*, *Mfge8*, *Sirpa*, *Cd72*, *Adgre1*, and *Ly6c2*) were also identified. These data suggest that exposure to 4NQO results in a substantial alteration of the leukocytes in the tongue epithelium, while the transcriptomic signature of certain mononuclear phagocytes implies the development of a tumor permissive environment.

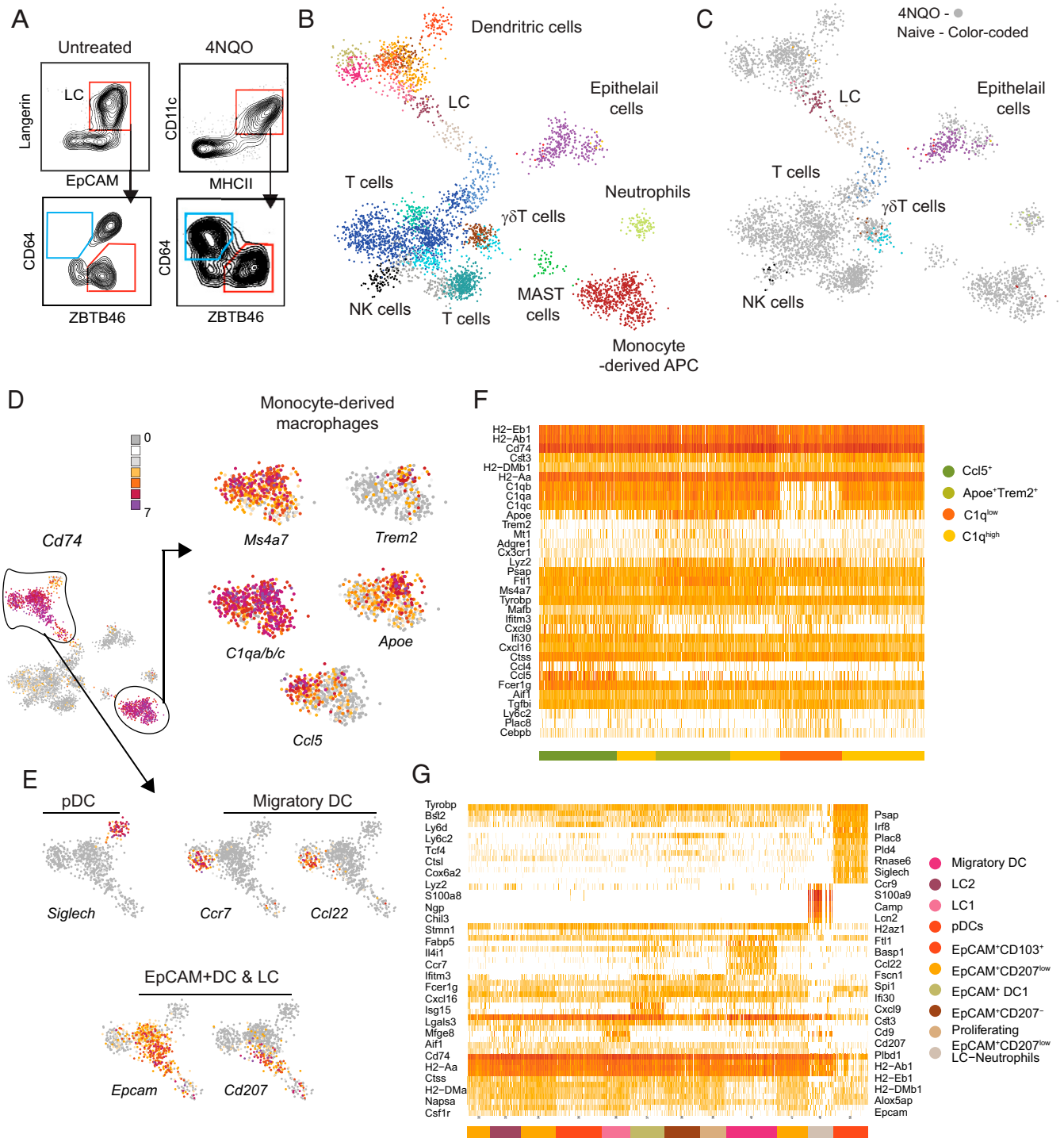

Fig. 6. Heterogeneous mononuclear phagocyte populations present in the tongue epithelium of 4NQO-treated mice. (*A*) *Zbtb46*^{gfp} mice were treated with 4NQO for 5 wk and the tongue epithelial layers were analyzed by flow cytometery. Representative flow cytometry plots show the expression of ZBTB46 and CD64 among the LC (naive) or APC (4NQO-treated mice) population. (*B–F*) CD45^{+} cells were enriched from a single-cell suspension prepared from the tongue epithelium of 4NQO-treated mice or naive mice and subjected to scRNAseq analysis. (*B*) Two-dimensional (2D) projection of the CD45^{+}-enriched cells in a color-coded fashion by major cell types. (*C*) Two-dimensional projection of the CD45^{+}-enriched cells of naive mice (color coded) overlaid on the cells enriched from 4NQO-treated mice (gray). (*D* and *E*) The 2D projection of a selected set of key genes related to monocyte-derived macrophages (*D*) and DCs (*E*) over the metacell model. (*F* and *G*) Heatmap depicting the z score of the most significantly differentiated genes in the cluster of monocyte-derived macrophages (*F*) and DCs (*G*).

The Epithelium following Chronic Exposure to 4NQO Is Enriched for Treg Cells. Besides myeloid cells, scRNAseq analysis revealed a diverse population of lymphocytes expressing the *Thy1* gene (Fig. 7 *A* and *B*). The majority of these cells express *Cd3e/d/g*, identifying them as T cells, whereas a smaller population was negative to CD3 yet expressed *Ncr1*, thus distinguished as NK cells. Among the T cells were a relatively small cluster of γδT cells (*Trgc1* and *Trdc*) that also express *Cd163l1* (*Scart1*),

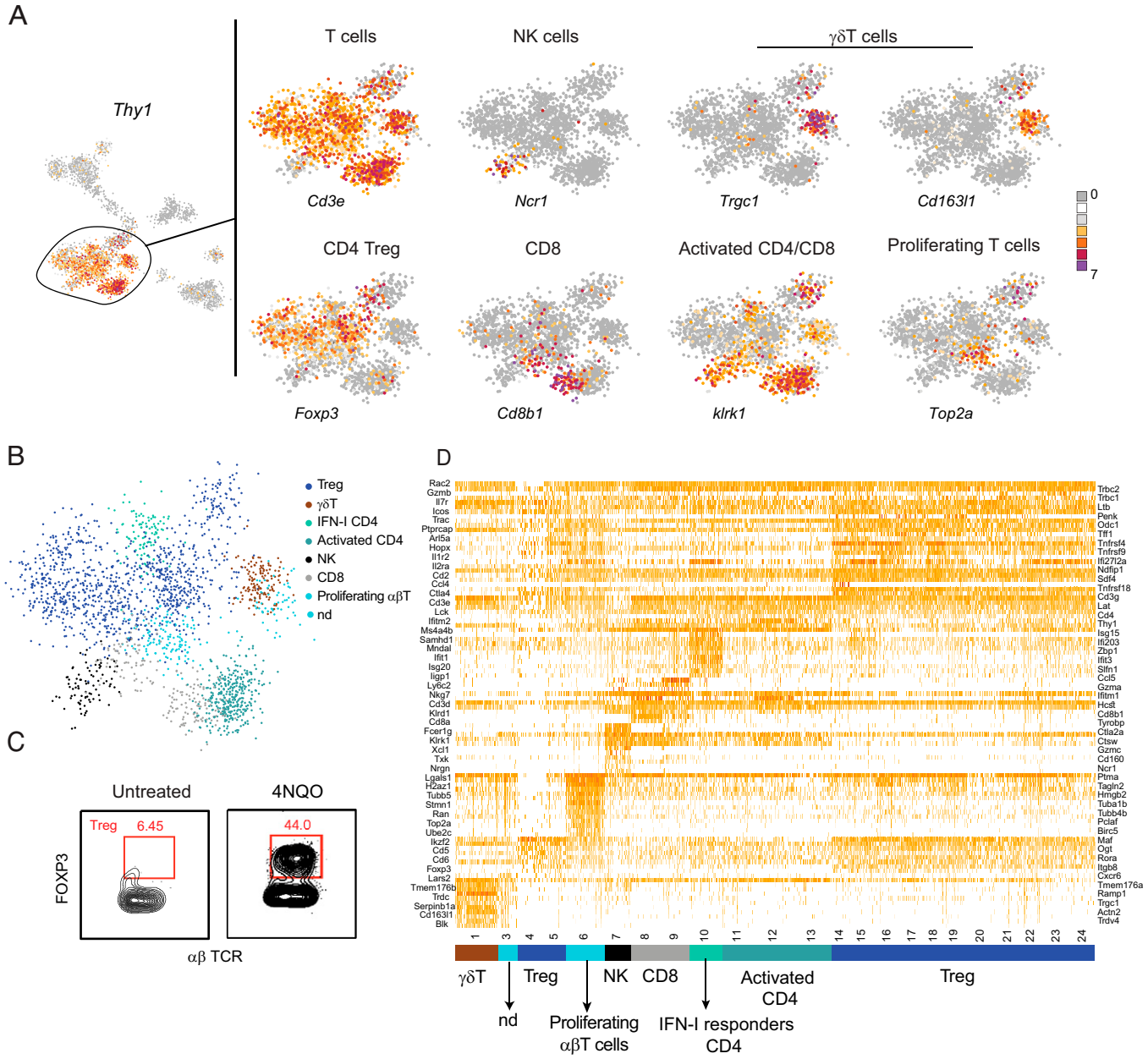

Fig. 7. Tregs are the main αβT cells in the tongue epithelium of prolonged 4NQO-treated mice. (*A*) Two-dimensional projection of a selected set of key genes related to the lymphocyte cluster over the metacell model. (*B*) Two-dimensional projection of the lymphocyte cluster in a color coded by main type of lymphocytes. (*C*) Representative flow cytometry plots show the percentages of FOXP3$^+$ αβT cells in the epithelium of naive mice and mice treated with 4NQO for 5 wk. (*D*) Heatmap depicting the z score of the most significantly differentiated genes in the lymphocyte cluster.

Tmem176a/b genes, *Cxcr6*, *Serpinb1a*, *Blk*, and *Actn2*, a signature representing tissue-resident effector γδT17 cells (38). Within the αβT cells, the majority of the cells express *Foxp3*, *Ctla4*, *Tnfrsf9*, *Tnfrsf4*, *Tnfrsf18*, *Rora*, *Il1r2*, *Icos*, and *Lgasl1*, in line with the signature of suppressive Treg cells (39). Flow cytometry analysis confirmed the presence of a large Treg population in the tongue epithelium at this time point, representing about 44% of the total αβT cells (Fig. 7*C*). In addition to the Treg cells, and concurring with our earlier observations demonstrating the presence of cytotoxic T cells, we detected activated CD4$^+$ and CD8$^+$ T cells in the epithelium. These cells express *Klrk1* (NKG2D), *Ctsw*, and *Nkg7*, indicating cytolytic activity (40), as well as *Cxcr6* that reported to be involved in T cell recruitment and retention in carcinoma (41). Some of the T cells express genes such as *Top2a*, *Hmgb2*, *Stmn1*, and *Birc5*, suggesting local proliferation. Taken together, besides altering the composition of mononuclear phagocytes in the tongue epithelium, exposure to 4NQO for 5 wk is also accompanied by an accumulation of lymphocytes, particularly Treg cells.

The Enrichment of Epithelial Treg Cells Is Regulated by pDCs. Human studies have previously highlighted an increase of tumor-infiltrating pDCs predicts a poor prognosis of OSCC and depletion of pDCs attenuates experimental OSCC (42, 43). Moreover, in various cancers, pDCs were associated with elevated levels of Treg cells in the tumor (44–48). To address the relationship between pDCs and Treg cells in the present experimental setting, we first characterized the kinetics of pDCs and Treg cells in the tongue epithelium and cervical LNs at various times after the 4NQO treatment. In both the tongue epithelium

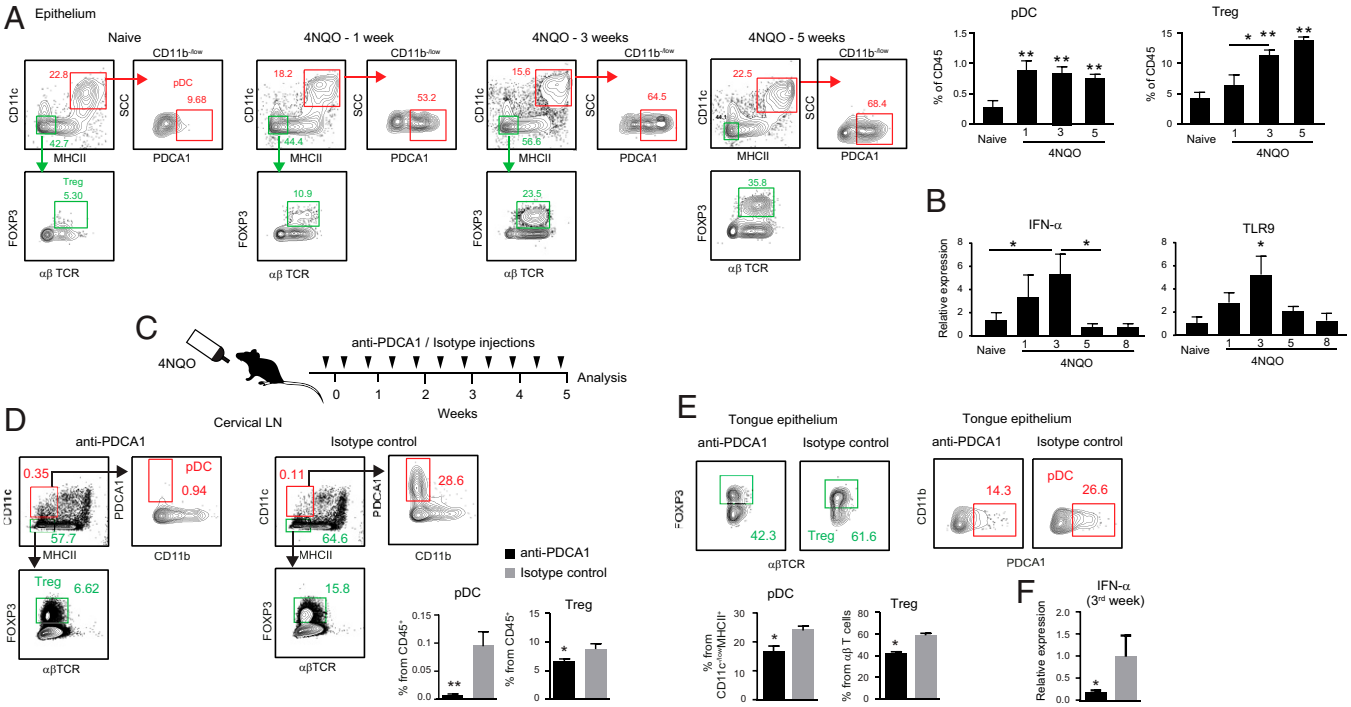

Fig. 8. pDCs contribute to the accumulation of Treg cells in the tongue epithelium. B6 mice were provided with 4NQO in the drinking water for 5 to 8 wk and tongue epithelial cells were collected for flow cytometry. (*A*) Representative flow cytometry plots and graph show the mean frequencies + SEM of pDCs ($CD45^+CD11c^+MHCII^+CD11b^{low}PDCA1^+$) and Treg cells ($CD45^+\alpha\beta TCR^+FOXP3^+$) in the noted weeks after 4NQO treatment ($n = 5$). Representative data are from two independent experiments. (*B*) Quantification by RT-PCR of the mean expression values + SEM of the noted genes in the tongue epithelium ($n = 5$). (*C–F*) Illustration depicting the administration of anti–PDCA-1 antibody or isotype control into mice treated with 4NQO for 3 wk. (*D*) Representative flow cytometry plots and graph present the mean percentages + SEM of pDCs and Treg cells in the cervical LNs ($n = 5$). (*E*) Representative plots and graph show the mean frequencies + SEM of Treg cells in the tongue epithelium ($n = 5$). (*F*) The levels of IFN-α mRNA in the tongue epithelium ($n = 5$). Representative data are from two independent experiments. $^*P < 0.05$. $^{**}P < 0.01$.

and LNs, the relative frequencies of the pDCs increase after 1 wk of treatment and remains high in the following weeks (Fig. 8*A* and *SI Appendix*, Fig. S7). Treg cells, on the other hand, were not detected in the first week, but after 3 to 5 wk of 4NQO treatment, their frequencies consistently increased. Since previous ex vivo studies suggest that pDCs isolated from human OSCC lose their capacity to produce IFN-α due to reduced TLR9 expression (42, 43, 49), we examined next the expression kinetics of both genes in the tongue epithelium. As depicted in Fig. 8*B*, both genes were significantly up-regulated 3 wk after the exposure to 4NQO but sharply reduced in the fifth week and later on. To examine directly the connection between pDCs and Tregs we treated mice with 4NQO and simultaneously depleted pDCs using an anti-PDCA1 monoclonal antibody or isotype control as illustrated in Fig. 8*C* and *SI Appendix*, Fig. S7*B*. Analysis of the LNs revealed that the pDCs were significantly depleted while the frequencies of the Tregs were partly but significantly reduced compared to mice receiving the isotype control (Fig. 8*D*). In the tongue epithelium, administration of anti-PDCA1 results in partial depletion of the pDCs but this was sufficient to reduce the frequencies of Treg cells by one-third (Fig. 8*E*). The depletion of pDCs also results in lower expression of IFN-α in the epithelium when the epithelium was analyzed after 3 wk of 4NQO treatment (Fig. 8*F*). These findings suggest that the presence of a large Treg population in the tongue epithelium is mediated, in part, by the pDCs.

Discussion

LCs are considered the sentinels of the epithelium; consistent with this notion, this study establishes a protective role of oral LCs in the early stages of carcinogen-induced OSCC. Nevertheless, constitutive exposure to the carcinogen 4NQO indirectly impairs the repopulation of resident LCs following their migration to the LNs to prime antitumor αβT cells, while at the same time numerous mononuclear phagocyte subtypes appear in the epithelium. This modification in the epithelial mononuclear phagocyte landscape was associated with the development of an immunosuppressive microenvironment within the tongue epithelium enabling the establishment of the tumor.

An early protective role was demonstrated for epidermal LCs during carcinogen-induced skin SCC, in which production of TNF-α by LCs induces the expression of CCL2 and CXCL10 in keratinocytes, resulting in rapid recruitment of NK cells (9). Such a mechanism was not observed here, likely due to the capacity of the carcinogen to down-regulate TNF-α signaling in oral epithelial cells. It is worth mentioning that, in humans, no differences were found in the frequencies of NK cells between healthy and OSCC patients, supporting the limited impact of these cells in oral malignancy (50). Besides the LC–NK cell axis, γδT cells were also reported to inhibit carcinogen-induced skin SCC via their capacity to express NKG2D, enabling elimination of keratinocytes expressing stress ligands (51, 52). While stress ligands were also up-regulated in our system, oral γδT cells do not express NKG2D and are dispensable for the early elimination of damaged $\gamma H2AX^+$ cells. This might be attributed, in part, to the distinct subsets of γδT cells residing in each epithelium. The epidermis is composed of $V\gamma5^+$ T cells, which are recognized to have cytotoxic activity, while the tongue epithelium is populated by the IL-17–producing $V\gamma6^+$ T cells that have been reported to exhibit both anti- and protumor capabilities (53). Taken together, NK and γδT cells are dispensable during the initiation of oral carcinogenesis, underlining the importance of LC-induced αβT cells in eliminating transformed cells

during the early stages of oral tumorigenesis. This is underlined by our finding that activated CD4/CD8$^+$ T cells expressing NKG2D were detected by scRNAseq analysis in carcinogen-treated tongues. Yet, while our study proposes an early protective role of LCs, by priming anticancer T cell immunity, LCs could also have other antitumor activities. For instance, the depletion of LCs could limit carcinogenicity, since LCs were reported to mediate carcinogen processing that facilitates DNA damage (10). It has also been proposed that LCs maintain tissue homeostasis by regulating gene expression in keratinocytes, thus their ablation might dysregulate tissue function and facilitate carcinogenesis (54).

While LCs were lost during 4NQO treatment, other mononuclear phagocyte populations develop in or are recruited to the tongue epithelium creating a compatible environment for tumor development. Among the DC population, a major subset expresses *Epcam*, consisting of a small subset of LCs (also expressing high *Cd207* levels), while the remainder expresses very low or negligible levels of *Cd207*. The latter are also capable of proliferating locally unlike steady-state oral LCs (4). Whereas 4NQO was not directly interfering with LC differentiation, its impact on the epithelial cells might cause this effect. Yet, the expression of TGF-β and BMP7, the cytokines driving the differentiation of oral LCs was not significantly altered by the carcinogen. We provided evidence that LC differentiation is likely regulated by the level of oxidative phosphorylation. This is in agreement with previous studies demonstrating that the development and function of LCs depend on mTORC1 signaling (55, 56), which also controls mitochondrial oxidative function (57). It is also possible that the inflammatory milieu generated in the epithelium dysregulates LC development (58). Indeed, under inflammatory conditions, monocytes infiltrate the skin epidermis and differentiate, in a TGF-β–independent manner, into inflammatory LCs expressing low levels of CD207 (59, 60). These inflammatory LCs were also shown to be short-lived, disappearing within 3 wk after the treatment, resembling the kinetics of LC repopulation in the current study upon the removal of 4NQO.

Other populations of mononuclear phagocytes residing in the 4NQO-treated epithelium include migratory DCs and pDCs. In this study, we demonstrated that pDCs accumulate during carcinogenesis together with Treg cells, while the frequencies of the latter were partly regulated by the pDCs. This is in agreement with previous clinical studies reporting a direct correlation between the numbers of tumor-infiltrating pDCs and the adverse outcome in primary OSCC patients (42). In this regard, pDCs were found to induce Treg cells through the ICOS/ICOS-L pathway and indoleamine 2,3-dioxygenase (IDO) expression (61). The reduced expression of TLR9 and IFN-α detected 5 wk after the exposure to 4NQO is also congruent with human observations (43, 49). Of note, the scRNAseq analysis indicates that pDCs express the highest level of *Irf8* among the various DC subsets, a phenotype associated with a reduced capacity to produce IFN-α (62). The reduction in IFN-α production was proposed to be mediated by the Treg cells via secretion of IL-10 and TGF-β, which potentially create a vicious cycle intensifying the immunosuppressive effect of the tumor (61, 63). Since in our system the depletion of pDCs results in partial reduction of the Treg cells, it is likely that other DCs besides pDCs control these cells. This could be mediated by the migratory DCs identified by the scRNAseq analysis, which express high levels of *Ccl22* and *Socs2*, an expression pattern promoting the development of Treg cells and further immune escape of tumor cells (36, 37). It is thus possible that the Treg cells are primed by CCL22-expressing DCs, whereas pDCs facilitate the local proliferation of the Treg cells.

Macrophages represent the other major mononuclear phagocyte population in the epithelium of 4NQO-treated mice, which our scRNAseq analysis provides several indications that these monocyte-derived cells might facilitate tumor development. For instance, a population of macrophages expresses *Apoe* and *Trem2*, which accumulating evidence suggests a role in promoting an immunosuppressive tumor microenvironment that also facilitates metastases (31, 33). Another subset expresses *Ccl5*, yet again associated with the capacity of macrophages to facilitate carcinogenesis and metastases (32). Moreover, all the macrophages express *Tgfbi*, reported for promoting tumor growth and has been associated with a poor prognosis of OSCC and ovarian cancer (17, 64, 65). The majority of the macrophages also express high levels of the complement *C1q* genes, which are implicated in the establishment of an immunosuppressive tumor microenvironment and poor prognosis in renal cell carcinoma (66). Additionally, the scRNAseq analysis in melanoma models identified a unique, dominant antiinflammatory macrophage population induced by Treg cells and defined by expression of the *C1q* gene (67).

In summary, this study demonstrates that oral LCs protect the host from epithelial carcinogenesis early, following exposure to the carcinogen. Nevertheless, prolonged exposure to the carcinogen dysregulates the differentiation of the mononuclear phagocytes in the oral epithelium, facilitating the development of immunosuppressive conditions that promote the establishment of the tumor. Our findings are in agreement with human data suggesting that oral malignancy is associated with reduced LC numbers (17), and the correlation of high LC numbers in the tumor microenvironment with a better prognosis (20, 21). Human studies have also reported a correlation between tumor-infiltrating pDCs and a poor prognosis of OSCC (42). Our data confirmed this observation and substantiate it by linking pDCs to the presence of Treg cells, which are also found in human OSCC (68, 69). We hope this study will encourage the development of novel diagnostic and therapeutic approaches for the detection and prevention of OSCC at its early stages.

Materials and Methods

Detailed information on antibodies, reagents, mice, and ethical approvals is described in *SI Appendix*. Details of the experimental OSCC setting, immunofluorescence staining, isolation, and processing of the murine tongue, conditional ablation of Langerhans cells, RNA extraction and RT-qPCR, single-cell RNA analysis of tongue leukocytes, RNAseq analysis of tongue epithelial cells, and statistical analysis are provided in *SI Appendix*. All animal protocols were approved by the Hebrew University Institutional Animal Care and Use Committee (IACUC).

Data Availability. Study data are available in the Gene Expression Omnibus (accession no. GSE192470). All other study data are included in the article and/or *SI Appendix*.

ACKNOWLEDGMENTS. This work was supported by the Israel Cancer Research Fund (Project Grant 2020 to A.-H.H.). The S.Y. laboratory is supported by the Israel Science Foundation (Awards 316/20 and 192/20).

1. J. Ali *et al.*, Genetic etiology of oral cancer. *Oral Oncol.* **70**, 23–28 (2017).
2. F. Bray *et al.*, Global cancer statistics 2018: GLOBOCAN estimates of incidence and mortality worldwide for 36 cancers in 185 countries. *CA Cancer J. Clin.* **68**, 394–424 (2018).
3. A. H. Hovav, Mucosal and skin Langerhans cells—Nurture calls. *Trends Immunol.* **39**, 788–800 (2018).
4. T. Capucha *et al.*, Distinct murine mucosal Langerhans cell subsets develop from pre-dendritic cells and monocytes. *Immunity* **43**, 369–381 (2015).
5. G. Hoeffel *et al.*, C-Myb(+) erythro-myeloid progenitor-derived fetal monocytes give rise to adult tissue-resident macrophages. *Immunity* **42**, 665–678 (2015).
6. G. Hoeffel *et al.*, Adult Langerhans cells derive predominantly from embryonic fetal liver monocytes with a minor contribution of yolk sac-derived macrophages. *J. Exp. Med.* **209**, 1167–1181 (2012).
7. T. Capucha *et al.*, Sequential BMP7/TGF-β1 signaling and microbiota instruct mucosal Langerhans cell differentiation. *J. Exp. Med.* **215**, 481–500 (2018).

8. H. K. Muller, G. M. Halliday, B. A. Knight, Carcinogen-induced depletion of cutaneous Langerhans cells. *Br. J. Cancer* **52**, 81–85 (1985).
9. D. Ortner *et al.*, Langerhans cells and NK cells cooperate in the inhibition of chemical skin carcinogenesis. *OncoImmunology* **6**, e1260215 (2016).
10. B. G. Modi *et al.*, Langerhans cells facilitate epithelial DNA damage and squamous cell carcinoma. *Science* **335**, 104–108 (2012).
11. J. Strid *et al.*, Acute upregulation of an NKG2D ligand promotes rapid reorganization of a local immune compartment with pleiotropic effects on carcinogenesis. *Nat. Immunol.* **9**, 146–154 (2008).
12. R. L. Albuquerque, Jr, M. C. Miguel, A. L. Costa, L. B. Souza, Correlation of c-erbB-2 and S-100 expression with the malignancy grading and anatomical site in oral squamous cell carcinoma. *Int. J. Exp. Pathol.* **84**, 259–265 (2003).
13. T. E. Daniels *et al.*, Reduction of Langerhans cells in smokeless tobacco-associated oral mucosal lesions. *J. Oral Pathol. Med.* **21**, 100–104 (1992).
14. T. J. Lasisi, A. O. Oluwasola, O. A. Lasisi, E. E. Akang, Association between Langerhans cells population and histological grade of oral squamous cell carcinoma. *J. Oral Maxillofac. Pathol.* **17**, 329–333 (2013).
15. P. D. Bittner-Eddy, L. A. Fischer, D. H. Kaplan, K. Thieu, M. Costalonga, Mucosal Langerhans cells promote differentiation of Th17 cells in a murine model of periodontitis but are not required for *Porphyromonas gingivalis*-driven alveolar bone destruction. *J. Immunol.* **197**, 1435–1446 (2016).
16. B. Narayanan, M. Narasimhan, Langerhans cell expression in oral submucous fibrosis: An immunohistochemical analysis. *J. Clin. Diagn. Res.* **9**, ZC39–ZC41 (2015).
17. Y. P. Wang *et al.*, Langerhans cell counts in oral epithelial dysplasia and their correlation to clinicopathological parameters. *J. Formos. Med. Assoc.* **116**, 457–463 (2017).
18. S. V. Rani *et al.*, Role of abnormal Langerhans cells in oral epithelial dysplasia and oral squamous cell carcinoma: A pilot study. *J. Nat. Sci. Biol. Med.* **6** (suppl. 1), S128–S133 (2015).
19. A. C. A. Pellicioli *et al.*, Immunosurveillance profile of oral squamous cell carcinoma and oral epithelial dysplasia through dendritic and T-cell analysis. *J. Oral Pathol. Med.* **46**, 928–933 (2017).
20. S. A. Goldman *et al.*, Peritumoral CD1a-positive dendritic cells are associated with improved survival in patients with tongue carcinoma. *Arch. Otolaryngol. Head Neck Surg.* **124**, 641–646 (1998).
21. N. Kindt *et al.*, Langerhans cell number is a strong and independent prognostic factor for head and neck squamous cell carcinomas. *Oral Oncol.* **62**, 1–10 (2016).
22. O. Gallo *et al.*, Langerhans cells related to prognosis in patients with laryngeal carcinoma. *Arch. Otolaryngol. Head Neck Surg.* **117**, 1007–1010 (1991).
23. T. Yilmaz, G. Gedikoglu, A. Celik, M. Onerci, E. Turan, Prognostic significance of Langerhans cell infiltration in cancer of the larynx. *Otolaryngol. Head Neck Surg.* **132**, 309–316 (2005).
24. B. L. Hawkins *et al.*, 4NQO carcinogenesis: A mouse model of oral cavity squamous cell carcinoma. *Head Neck* **16**, 424–432 (1994).
25. R. Czerninski, P. Amornphimoltham, V. Patel, A. A. Molinolo, J. S. Gutkind, Targeting mammalian target of rapamycin by rapamycin prevents tumor progression in an oral-specific chemical carcinogenesis model. *Cancer Prev. Res. (Phila.)* **2**, 27–36 (2009).
26. Z. Liu *et al.*, Fate mapping via Ms4a3-expression history traces monocyte-derived cells. *Cell* **178**, 1509–1525.e1519 (2019).
27. A. T. Satpathy *et al.*, Zbtb46 expression distinguishes classical dendritic cells and their committed progenitors from other immune lineages. *J. Exp. Med.* **209**, 1135–1152 (2012).
28. X. Wu *et al.*, Mafb lineage tracing to distinguish macrophages from other immune lineages reveals dual identity of Langerhans cells. *J. Exp. Med.* **213**, 2553–2565 (2016).
29. I. Sandrock *et al.*, Genetic models reveal origin, persistence and non-redundant functions of IL-17-producing γδ T cells. *J. Exp. Med.* **215**, 3006–3018 (2018).
30. Y. Baran *et al.*, MetaCell: Analysis of single-cell RNA-seq data using K-nn graph partitions. *Genome Biol.* **20**, 206 (2019).
31. A. Deczkowska, A. Weiner, I. Amit, The physiology, pathology, and potential therapeutic applications of the TREM2 signaling pathway. *Cell* **181**, 1207–1217 (2020).
32. R. Huang *et al.*, CCL5 derived from tumor-associated macrophages promotes prostate cancer stem cells and metastasis via activating β-catenin/STAT3 signaling. *Cell Death Dis.* **11**, 234 (2020).
33. P. Zheng *et al.*, Tumor-associated macrophages-derived exosomes promote the migration of gastric cancer cells by transfer of functional Apolipoprotein E. *Cell Death Dis.* **9**, 434 (2018).
34. M. O. Kim, S. J. Yun, I. S. Kim, S. Sohn, E. H. Lee, Transforming growth factor-beta-inducible gene-h3 (beta(ig)-h3) promotes cell adhesion of human astrocytoma cells in vitro: Implication of alpha6beta4 integrin. *Neurosci. Lett.* **336**, 93–96 (2003).
35. H. Tomioka, K. Morita, S. Hasegawa, K. Omura, Gene expression analysis by cDNA microarray in oral squamous cell carcinoma. *J. Oral Pathol. Med.* **35**, 206–211 (2006).
36. C. J. Nirschl *et al.*, IFNγ-dependent tissue-immune homeostasis is co-opted in the tumor microenvironment. *Cell* **170**, 127–141.e15 (2017).
37. M. Rapp *et al.*, CCL22 controls immunity by promoting regulatory T cell communication with dendritic cells in lymph nodes. *J. Exp. Med.* **216**, 1170–1181 (2019).
38. L. Tan *et al.*, Single-cell transcriptomics identifies the adaptation of Scart1^{+} Vγ6^{+} T cells to skin residency as activated effector cells. *Cell Rep.* **27**, 3657–3671.e4 (2019).
39. R. J. Miragaia *et al.*, Single-cell transcriptomics of regulatory T cells reveals trajectories of tissue adaptation. *Immunity* **50**, 493–504.e7 (2019).
40. S. S. Ng *et al.*, The NK cell granule protein NKG7 regulates cytotoxic granule exocytosis and inflammation. *Nat. Immunol.* **21**, 1205–1218 (2020).
41. G. Parsonage *et al.*, CXCR6 and CCR5 localize T lymphocyte subsets in nasopharyngeal carcinoma. *Am. J. Pathol.* **180**, 1215–1222 (2012).
42. N. Han *et al.*, Increased tumor-infiltrating plasmacytoid dendritic cells predicts poor prognosis in oral squamous cell carcinoma. *Arch. Oral Biol.* **78**, 129–134 (2017).
43. E. Hartmann *et al.*, Identification and functional analysis of tumor-infiltrating plasmacytoid dendritic cells in head and neck cancer. *Cancer Res.* **63**, 6478–6487 (2003).
44. C. Conrad *et al.*, Plasmacytoid dendritic cells promote immunosuppression in ovarian cancer via ICOS costimulation of Foxp3(+) T-regulatory cells. *Cancer Res.* **72**, 5240–5249 (2012).
45. J. Faget *et al.*, ICOS-ligand expression on plasmacytoid dendritic cells supports breast cancer progression by promoting the accumulation of immunosuppressive CD4+ T cells. *Cancer Res.* **72**, 6130–6141 (2012).
46. X. M. Huang *et al.*, Role of plasmacytoid dendritic cells and inducible costimulator-positive regulatory T cells in the immunosuppression microenvironment of gastric cancer. *Cancer Sci.* **105**, 150–158 (2014).
47. A. Pedroza-Gonzalez *et al.*, Tumor-infiltrating plasmacytoid dendritic cells promote immunosuppression by Tr1 cells in human liver tumors. *OncoImmunology* **4**, e1008355 (2015).
48. L. L. Yang *et al.*, pDC depletion induced by CD317 blockade drives the antitumor immune response in head and neck squamous cell carcinoma. *Oral Oncol.* **96**, 131–139 (2019).
49. N. Han *et al.*, Culture supernatants of oral cancer cells induce impaired IFN-α production of pDCs partly through the down-regulation of TLR-9 expression. *Arch. Oral Biol.* **93**, 141–148 (2018).
50. O. Stasikowska-Kanicka, M. Wągrowska-Danilewicz, M. Danilewicz, Association of infiltrating cells with microvessel density in oral squamous cell carcinoma. *Pol. J. Pathol.* **68**, 40–48 (2017).
51. M. Girardi *et al.*, Resident skin-specific gammadelta T cells provide local, nonredundant regulation of cutaneous inflammation. *J. Exp. Med.* **195**, 855–867 (2002).
52. M. Girardi *et al.*, Regulation of cutaneous malignancy by gammadelta T cells. *Science* **294**, 605–609 (2001).
53. B. Silva-Santos, K. Serre, H. Norell, γδ T cells in cancer. *Nat. Rev. Immunol.* **15**, 683–691 (2015).
54. Q. Su *et al.*, Brief communication: Long-term absence of Langerhans cells alters the gene expression profile of keratinocytes and dendritic epidermal T cells. *PLoS One* **15**, e0223397 (2020).
55. B. Kellersch, T. Brocker, Langerhans cell homeostasis in mice is dependent on mTORC1 but not mTORC2 function. *Blood* **121**, 298–307 (2013).
56. F. Sparber *et al.*, The late endosomal adaptor molecule p14 (LAMTOR2) represents a novel regulator of Langerhans cell homeostasis. *Blood* **123**, 217–227 (2014).
57. J. T. Cunningham *et al.*, mTOR controls mitochondrial oxidative function through a YY1-PGC-1alpha transcriptional complex. *Nature* **450**, 736–740 (2007).
58. J. Yao *et al.*, Single-cell transcriptomic analysis in a mouse model deciphers cell transition states in the multistep development of esophageal cancer. *Nat. Commun.* **11**, 3715 (2020).
59. F. Ginhoux *et al.*, Langerhans cells arise from monocytes in vivo. *Nat. Immunol.* **7**, 265–273 (2006).
60. K. Seré *et al.*, Two distinct types of Langerhans cells populate the skin during steady state and inflammation. *Immunity* **37**, 905–916 (2012).
61. V. Koucký, J. Bouček, A. Fialová, Immunology of plasmacytoid dendritic cells in solid tumors: A brief review. *Cancers (Basel)* **11**, 470 (2019).
62. D. Sichien *et al.*, IRF8 transcription factor controls survival and function of terminally differentiated conventional and plasmacytoid dendritic cells, respectively. *Immunity* **45**, 626–640 (2016).
63. W. Vermi, M. Soncini, L. Melocchi, S. Sozzani, F. Facchetti, Plasmacytoid dendritic cells and cancer. *J. Leukoc. Biol.* **90**, 681–690 (2011).
64. S. V. Puram *et al.*, Single-cell transcriptomic analysis of primary and metastatic tumor ecosystems in head and neck cancer. *Cell* **171**, 1611–1624.e1624 (2017).
65. A. M. Steitz *et al.*, Tumor-associated macrophages promote ovarian cancer cell migration by secreting transforming growth factor beta induced (TGFBI) and tenascin C. *Cell Death Dis.* **11**, 249 (2020).
66. L. T. Roumenina *et al.*, Tumor cells hijack macrophage-produced complement C1q to promote tumor growth. *Cancer Immunol. Res.* **7**, 1091–1105 (2019).
67. C. Liu *et al.*, Treg cells promote the SREBP1-dependent metabolic fitness of tumor-promoting macrophages via repression of CD8^{+} T cell-derived interferon-γ. *Immunity* **51**, 381–397.e6 (2019).
68. S. Aggarwal, S. C. Sharma, S. N Das, Dynamics of regulatory T cells (T_{regs}) in patients with oral squamous cell carcinoma. *J. Surg. Oncol.* **116**, 1103–1113 (2017).
69. K. P. Lim *et al.*, CD4+CD25hiCD127low regulatory T cells are increased in oral squamous cell carcinoma patients. *PLoS One* **9**, e103975 (2014).